AGU ADVANCING EARTH AND SPACE SCIENCES

Geophysical Research Letters®

RESEARCH LETTER
10.1029/2023GL104905

Key Points:

- Parallel electron beam-mode waves are modulated by whistler near the current sheet mid-plane, by driving beams through Landau resonance
- Electron beam-mode and cyclotron waves are modulated by lower-hybrid waves near separatrices, with beam and loss cone distributions

Correspondence to:

S. Wang,
coralwang90@gmail.com

Citation:

Wang, S., Graham, D. B., An, X., Li, L., Zong, Q.-G., Zhou, X.-Z., et al. (2023). Electrostatic waves around a magnetopause reconnection secondary electron diffusion region modulated by whistler and lower-hybrid waves. *Geophysical Research Letters*, *50*, e2023GL104905. https://doi.org/10.1029/2023GL104905

Received 12 JUN 2023
Accepted 28 AUG 2023

Author Contributions:

Conceptualization: Shan Wang, Qiu-Gang Zong
Formal analysis: Shan Wang, Daniel B. Graham, Li Li
Investigation: Shan Wang, Daniel B. Graham, Xin An, Li Li
Methodology: Shan Wang
Software: Shan Wang
Validation: Li Li
Visualization: Shan Wang, Qiu-Gang Zong, Xu-Zhi Zhou
Writing – original draft: Shan Wang
Writing – review & editing: Daniel B. Graham, Xin An, Li Li, Qiu-Gang Zong, Xu-Zhi Zhou, Wen-Ya Li, Zhi-Yang Liu

Electrostatic Waves Around a Magnetopause Reconnection Secondary Electron Diffusion Region Modulated by Whistler and Lower-Hybrid Waves

Shan Wang[1], Daniel B. Graham[2], Xin An[3], Li Li[1], Qiu-Gang Zong[1,4], Xu-Zhi Zhou[1], Wen-Ya Li[5], and Zhi-Yang Liu[1]

[1]Institute of Space Physics and Applied Technology, Peking University, Beijing, China, [2]Swedish Institute of Space Physics, Uppsala, Sweden, [3]Department of Earth, Planetary, and Space Sciences, University of California, Los Angeles, CA, USA, [4]State Key Laboratory of Lunar and Planetary Sciences, Macau University of Science and Technology (MUST), Taipa, China, [5]State Key Laboratory of Space Weather, National Space Science Center, Chinese Academy of Sciences, Beijing, China

Abstract We investigate electrostatic waves in a magnetopause reconnection event around a secondary electron diffusion region. Near the current sheet mid-plane, parallel electron beam-mode waves are modulated by whistler waves. We conclude that the anisotropy of energized electrons in the reconnection exhaust excites whistler waves, which produce spatially modulated electron beams through nonlinear Landau resonance, and these beams excite beam-mode electrostatic waves. In the separatrix region, parallel propagating electrostatic waves associated with field-aligned electron beams and perpendicular propagating electron cyclotron harmonic waves with loss cone distributions exhibit modulation frequencies in the lower-hybrid wave (LHW) frequency range. We infer that LHWs scatter electrons to produce beams and alter loss cones to modulate electrostatic waves. The results advance our understanding about the regimes and mechanisms of electrostatic waves in reconnection, with an emphasis on their coupling with lower-frequency electromagnetic waves.

Plain Language Summary Magnetic reconnection is an important energy dissipation process at the Earth's dayside magnetopause. In its central region, plasmas deviate from the thermal equilibrium and form structured distribution functions, which excite plasma waves. We investigate high-frequency electrostatic waves in an event, where the waves are associated with electron beam—plasma interaction or anisotropy of distribution functions. We find that electrostatic waves are driven and modulated by lower-frequency waves, as the latter alters the particle distribution functions. The results help us understand how various processes couple with each other to achieve the energy dissipation.

1. Introduction

Magnetic reconnection explosively converts energies from electromagnetic fields to plasmas. Highly structured non-Maxwellian distributions are created in reconnection, which can be unstable to a variety of plasma waves that further interact with particles, so waves may be potential pathways of achieving the energy dissipation in reconnection.

Quasi-electrostatic waves at the electron Debye length (D_e) scale are ubiquitous plasma phenomena, and the responsible excitation mechanisms are often associated with beam-plasma interactions, for example, an electron beam drifting with respect to background electrons and ions. For one-dimensional electrostatic waves in unmagnetized (or field-aligned) plasmas with multiple populations, the dispersion relation is (modified from Equation 8.4.18 in Gurnett and Bhattacharjee (2005)):

$$1 - \frac{1}{2}\sum_s \frac{\omega_{\mathrm{ps}}^2}{k^2 v_{\mathrm{ts}}^2} Z'(\zeta^s) = 0 \tag{1}$$

where for each species s, ω_{ps} is the plasma frequency, $v_{ts} = \sqrt{2T_s/m_s}$ is the thermal speed, Z' is the derivative of the plasma dispersion function, $\zeta^s = (\omega - kV_s)/(kv_{\mathrm{ts}})$, and V_s is the bulk velocity. For populations with $|\zeta^s| \gg 1$, the contribution to Equation 1 is of the cold beam type $\sim \frac{\omega_{ps}^2}{(\omega - kV_s)^2}$ or with thermal corrections such as in Langmuir waves $\sim \frac{\omega_{\mathrm{ps}}^2}{(\omega - kV_s)^2}\left[1 + \frac{3k^2 v_{\mathrm{ts}}^2}{2(\omega - kV_s)^2}\right]$. For $|\zeta^s| \ll 1$, the term is $\sim \frac{\omega_{\mathrm{ps}}^2}{3k^2 v_{\mathrm{ts}}^2}$, such as for hot electrons in ion/electron acoustic

waves. The Langmuir wave has $\omega \geq \omega_{pe}$, and it tends to be the dominant mode if the beam is weak and suprathermal (An et al., 2019; Lu et al., 2005; Omura et al., 1996). The beam or acoustic modes often have $\omega < \omega_{pe}$, though occasions exist in the Earth's magnetosphere regime where $\omega > \omega_{pe}$ (Fuselier et al., 1985). When the electron beam speed is comparable to the background electron thermal speed ($V_{beam} \sim v_{te,bg}$), it tends to excite instabilities through electron-electron interactions, and the resulting wave has high frequencies ($\omega \gg \omega_{pi}$) and high phase speeds (V_{ph}) comparable to $v_{te,bg}$; a slow electron beam ($V_{beam} \ll v_{te,bg}$) tends to excite waves through electron-ion interactions, and the resulting Buneman-like or ion acoustic-like waves have low frequencies ($\omega \lesssim \omega_{pi}$) and low V_{ph} (Graham et al., 2016; Norgren et al., 2015). Such quasi-parallel waves are commonly observed in reconnection regions (e.g., Khotyaintsev et al., 2019 and references therein), which may trap particles and thermalize distributions (e.g., Khotyaintsev et al., 2020). For quasi-perpendicular waves, non-gyrotropic electron distributions in the electron diffusion region (EDR) may excite upper hybrid waves (e.g., Burch et al., 2019; Graham et al., 2017; Jiang et al., 2019) and electron Bernstein waves (e.g., W.-Y. Li et al., 2020), which may alter the distributions, pressure and potentially the reconnection electric field (Dokgo et al., 2020a, 2020b; W-Y. Li et al., 2020, 2021).

Waves at higher frequencies may be modulated by those at lower-frequencies, a way to cause energy transfer across scales. For example, inside the magnetosphere, ultra-low-frequency waves may modulate electromagnetic-ion-cyclotron waves (e.g., Liu et al., 2022), whistler and electron cyclotron harmonic (ECH) waves (e.g., Zhang et al., 2019); kinetic Alfven waves may modulate time domain structures around injection fronts (An et al., 2021). Whistler waves with oblique propagations may produce parallel beams that may further drive Langmuir or electron acoustic waves (An et al., 2019), observed in magnetopause reconnection (J. Li et al., 2018) as well as other environments like the radiation belts (J. Li et al., 2017) and foreshock (Wang et al., 2020).

During magnetopause reconnection, electrostatic waves are commonly observed and they are capable of penetrating to the central EDR region, for example, statistical results by Wilder et al. (2019). However, there still lacks a systematic picture about what regimes of electrostatic waves are applicable in each reconnection sub-region, and whether and how they are coupled with other waves. Using observations by the Magnetosphere Multiscale (MMS) mission, we find rich electrostatic waves around a secondary EDR event at magnetopause. We analyze the wave properties and corresponding plasma conditions, with an emphasis on the electrostatic waves modulated by lower-frequency waves, trying to advance the comprehension of the questions above.

2. Data

Data are from MMS burst-mode measurements. The magnetic fields are from the Flux Gate Magnetometer at 128 samples/s (Russell et al., 2016) and Search Coil Magnetometer at 8,192 samples/s (Le Contel, Leroy, Roux et al., 2016). Electric fields are from the double probes at 8,192 samples/s (Ergun et al., 2016; Lindqvist et al., 2016; Torbert et al., 2016), where the DC-coupled "dce" product has 8,192 samples/s and the AC-coupled "hmfe" product that have fewer available intervals than "dce" data has 65,536 samples/s. Plasma data are from the Fast Plasma Investigation (Pollock et al., 2016), where the ion and electron measurements have time resolutions of 0.15 and 0.03 s, respectively.

3. Observations

3.1. Overview of the Context and Waves in the Event

The event was on 26 February 2018 (Figure 1). MMS crossed the magnetopause reconnection current sheet with B_L reversals (Figure 1b), where $B_L > 0$ indicates the magnetospheric side. The LMN coordinate is determined by Minimum Variance Analysis on magnetic fields during 09:52:04.4–09:52:07.1 UT, where L = [−0.3561, −0.2697, 0.8946], M = [−0.2353, −0.9007, −0.3652], and N = [0.9043, −0.3406, 0.2593] in GSM. Overall the spacecraft was in a reconnection exhaust with large $V_{iL} > 0$ (Figure 1c) and dense magnetosheath-origin electrons dominate the spectrogram (Figure 1a). Around 09:52:08 UT, a strong positive V_{eM} (Figure 1d) was observed by MMS1. The associated V_{eL} reversal indicates a possible crossing from the +L to −L sides of an X-line. MMS3 was located on the more magnetospheric side than MMS1 with more positive B_L (gray in Figure 1b), and it was more on the +L side, since it observed $V_{eL} > 0$ (Figure 1e) when MMS1 observed $V_{eL} < 0$. Electron distributions (Figures 1h and 1i) show that MMS1 observed non-gyrotropic (asymmetric along $v_{\perp 1}$ with respect to the bulk velocity) electron beams with $v_{\parallel} < 0$ at the negative V_{eL} peak (A), while MMS3 observed non-gyrotropic (slanted

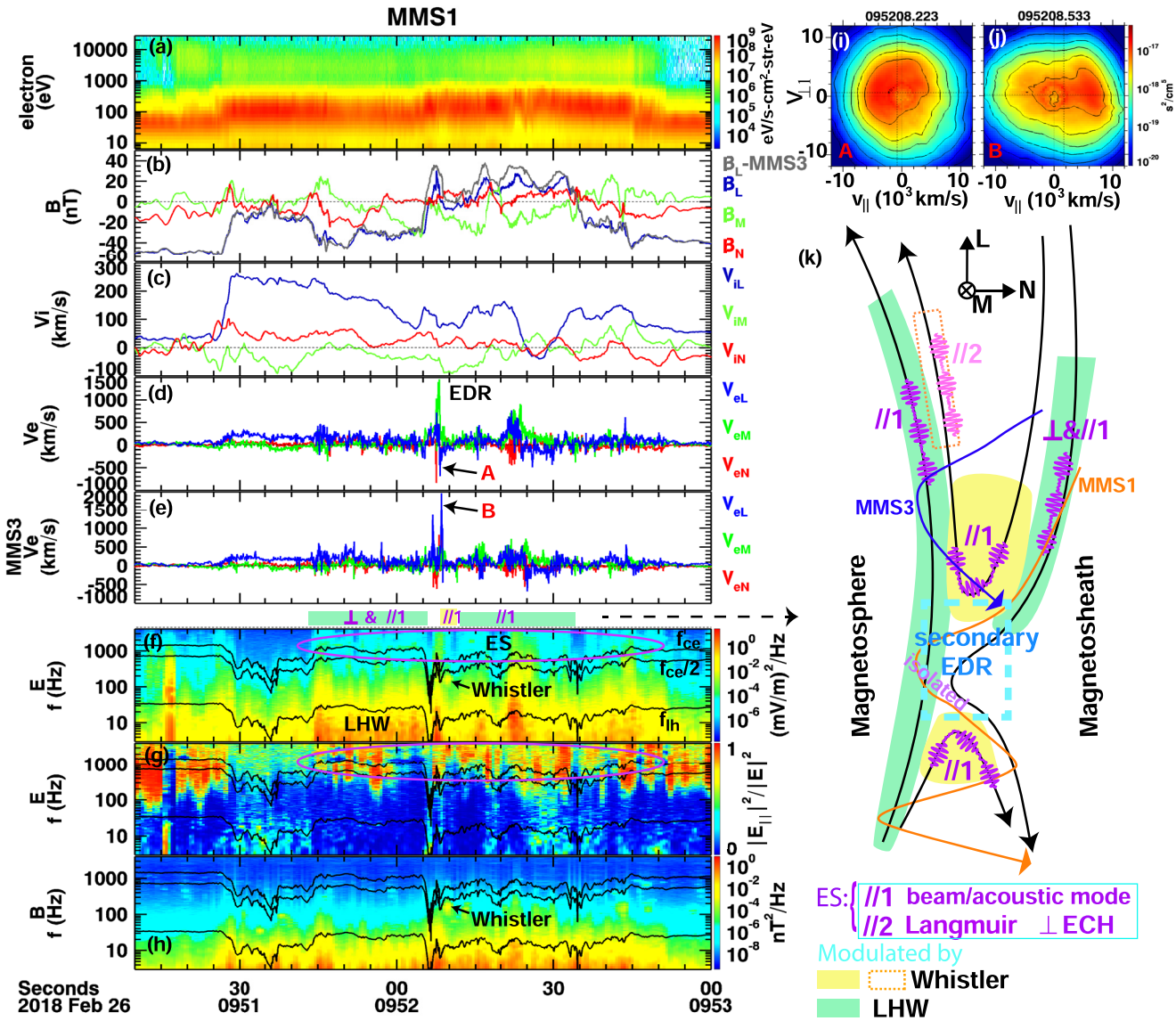

Figure 1. Overview of the event. Quantities without labels of the spacecraft number are from MMS1, and B_L and V_e from MMS3 are provided in (b) and (e), respectively. (a) Electron spectrogram; (b) magnetic field; (c) ion velocity; (d) electron velocity from MMS1; (e) electron velocity from MMS3. (f) ***E*** power spectrum; (g) $|E_\parallel|^2/|E|^2$; (h) ***B*** power spectrum. (i) Electron distribution at the negative V_{eL} peak (location A marked in (d)) observed by MMS1; (j) Electron distribution at the positive V_{eL} peak (location B marked in (e)) observed by MMS3. (k) Illustrative summary of electrostatic waves in magnetopause reconnection and spacecraft trajectories. Repeated wave packets indicate modulations electrostatic waves by whistler or lower-hybrid waves.

shape) beams with $v_\parallel > 0$ at the positive V_{eL} peak (B). The beams are magnetosheath origin electrons that move toward the magnetospheric side. The distributions further support the encounter of a secondary EDR (embedded in a primary reconnection outflow) with a break of the magnetic field topology, electron demagnetization, and electron energization. According to these signatures, the spacecraft trajectories are illustrated in Figure 1j.

The event has rich wave activities as seen in the FFT power spectra of electric (Figure 1f) and magnetic fields (Figure 1h). Lower-hybrid waves (LHWs) are observed with electromagnetic fluctuations mainly below the lower-hybrid frequency (f_{lh}), with occasions extending much above f_{lh}. The wave power is strongest where B_L has large positive values and V_{eM} is strong, indicating the close vicinity to the density gradient near the magnetospheric separatrix/boundary of the EDR current sheet. LHWs are possibly also excited near the magnetosheath side separatrix with large negative B_L, and the wave fields penetrate to the current sheet mid-plane with small $|B_L|$, where the wave is weaker (e.g., around 09:51:30 and 09:52:30 UT). In this study, we refer to whistler waves as the narrow-band enhancement slightly below $f_{ce}/2$ (marked in Figures 1f and 1h) close to the current sheet mid-plane.

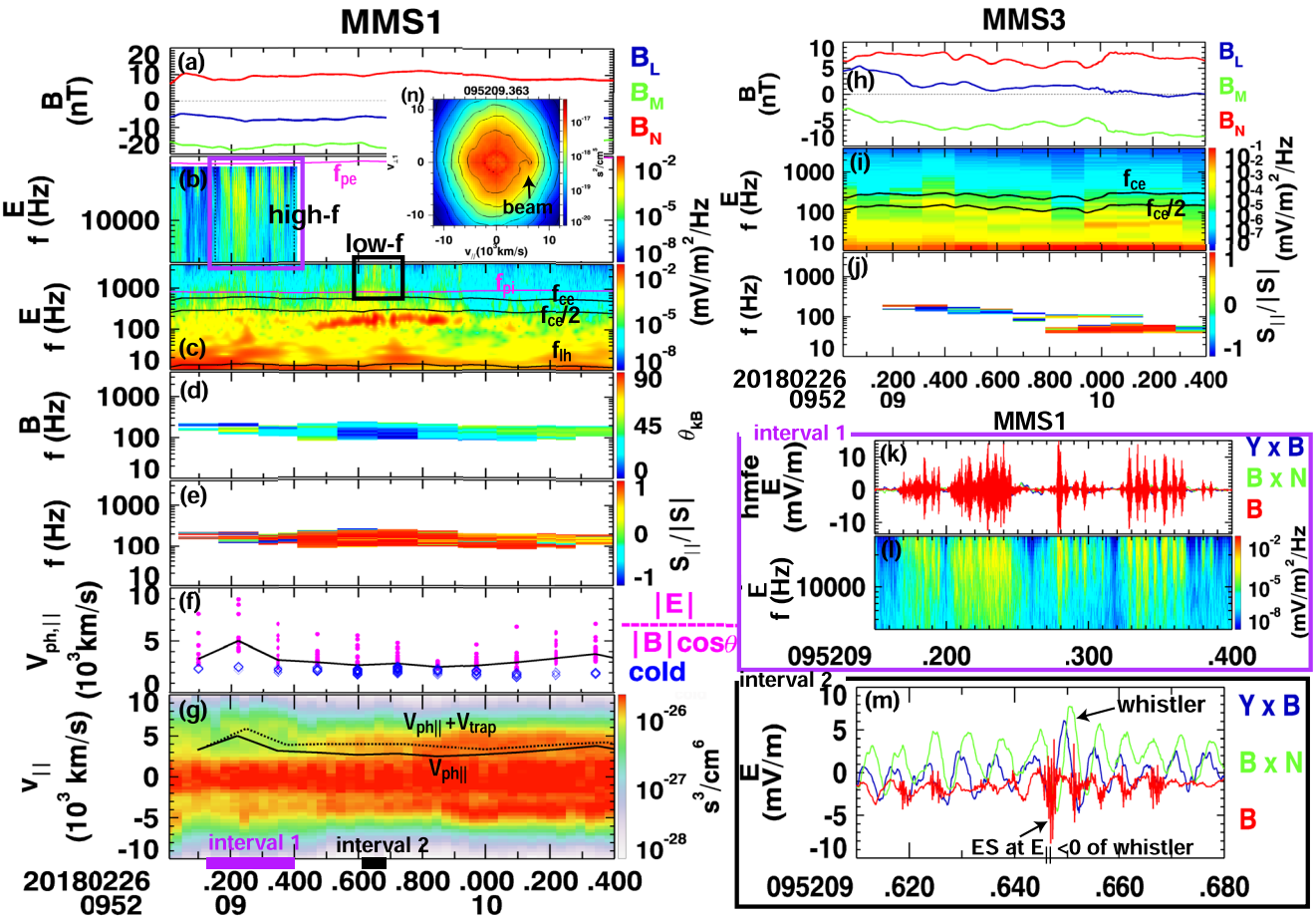

Figure 2. Parallel electrostatic waves (beam/acoustic mode below f_{pe}) modulated by whistler waves near the current sheet mid-plane. MMS1 was on the magnetosheath side with $B_L < 0$ (a). It observed whistler waves slightly below $f_{ce}/2$ and electrostatic waves at $f_{pi} < f < f_{pe}$ seen in the electric field wave power spectrum (b and c). The wave normal angle for selected whistler wave bins has small values (d and e). The parallel Poynting flux is mostly positive; (f) estimated parallel phase speed ($V_{ph||}$) of whistler, magenta: $|E|/(|B|\cos\theta_{kB})$, black: median of magenta dots, blue: theoretical values in the cold plasma limit. (g) Electron $v_{||}$ spectrogram, showing holes near the whistler $V_{ph||}$ (black solid curve), also seen in the 2D distribution in (n). The overplotted dashed curve is $V_{ph||} + V_{trap}$, where V_{trap} is the trapping velocity by the potential of whistler $E_{||}$, which approaches to the beam velocity. (h–j) Magnetic field, electric field wave power spectrum, and the parallel Poynting flux from MMS3, showing that whistler also exists at $B_L > 0$. (k and l) Example waveform and power spectrum of modulated electrostatic waves slightly below f_{pe} for interval 1 marked at the bottom of left panels. (m) Example waveform in interval 2 showing electrostatic waves slightly above f_{pi} occurring at the negative $E_{||}$ phase of whistler.

Our focus is the electrostatic wave mainly above $f_{ce}/2$ with the power enhancements marked by a purple oval. On the magnetospheric side ($B_L > 0$, e.g., 09:52:10–09:52:30 UT), quasi-parallel waves dominate with $|E_{||}|^2/|E|^2$ close to unity (Figure 1g). On the magnetosheath side ($B_L < 0$, e.g., 09:51:40–09:52:05 UT), bands of perpendicular waves ($|E_{||}|^2/|E|^2 \sim 0$) are present slightly above f_{ce}, co-existing with parallel waves.

3.2. Parallel Electron Beam Mode Waves in Whistler

A series of electrostatic waves are present and modulated in the whistler wave in the vicinity of the current sheet mid-plane ($B_L \sim 0$, Figures 2a and 2h). Whistler observed by MMS1 occurs at $B_L < 0$ with frequencies slightly below $f_{ce}/2$ (Figure 2c), associated with the perpendicular anisotropy of energized magnetosheath electrons (seen in Figure 2n) slightly downstream of the central EDR (Wang et al., 2022). We select whistler waves as bins in FFT spectrograms that have magnetic field powers >10 times of the background noise level, degree of polarization >0.7, and ellipticity >0.5 (using the spectral analysis (Samson & Olson, 1980)). The wave normal angle from the magnetic field spectral analysis is overall smaller than 45° with an average value of ~30° (Figure 2d). The parallel Poynting flux for the identified whistler waves is positive at MMS1 (Figure 2e), indicating a propagation away from the mid-plane toward the magnetosheath side (referring to Figure 1k for illustrations of magnetic field

directions). During the same interval, MMS3 observed whistler waves at $B_L \geq 0$, and the parallel Poynting flux exhibits both positive and negative values, indicating the close proxy to the wave source region (Figures 2h–2j).

Enhancements of high-frequency electrostatic wave powers (Figures 2b and 2c) lie in $f_{pi} < f < f_{pe}$, with the peak power sometimes slightly below f_{pe} such as around 09:52:09.15–09:52:09.40 UT and sometimes just above f_{pi} such as around 09:52:09.6 UT (the peak power ~3,000 Hz is well resolved). The zoom-in plots (Figures 2k–2m) show that the electrostatic waves are mainly along $E_{||}$ and the occurrence is clearly modulated by whistler. For example, eight wave packets occur during an interval of 0.05 s from 09:52:09.32 to 09:52:09.37 UT, corresponding to a modulation frequency of 160 Hz, equal to the whistler frequency. Figure 2m further shows that the electrostatic wave occurs at the negative $E_{||}$ phase of whistler, a feature consistent with the secondary wave produced by an oblique whistler with $V_{ph||} > 0$ (e.g., An et al., 2019; J. Li et al., 2018). Electrons with velocities close to $V_{ph||}$ can be trapped by whistler through nonlinear Landau resonance. The trapped population gets accelerated toward larger $v_{||}$ during the negative $E_{||}$ phase, forming a beam to trigger secondary instabilities.

The above scenario is more quantitatively supported by wave properties and electron distribution features. For selected whistler bins in Figures 2d and 2e, we estimate $V_{ph||}$ using $\frac{|E|}{|B|\cos\theta_{kB}}$ (magenta dots in Figure 2f) with the median values at each time shown with a black curve. The values are 3,000–5,000 km/s, slightly larger than those from the cold plasma dispersion relation ($V_{ph||} = \sqrt{\frac{\omega(\Omega_{ce}\cos\theta_{kB}-\omega)}{\omega_{pe}^2}}$) of 2,000–2,500 km/s (blue diamonds). The electron $v_{||}$ spectrogram (Figure 2g) exhibits holes between background and beams around the estimated median values of $V_{ph||}$ at 09:52:09.2–09:52:09.4 UT, also seen in the 2D distribution (Figure 2n). Beam speeds oscillate, which indicates possible modulations by whistler, though data resolution is not sufficient to fully resolve the whistler-frequency signature. We further estimate the trapping velocity due to the potential of whistler $E_{||}$ (Φ) using $V_{trap} = \sqrt{\frac{2e\Phi}{m_e}} \approx 2\sqrt{\frac{eE_{||0}}{m_e k_{||}}}$, where $E_{||0}$ is the amplitude of whistler $E_{||}$ obtained from the FFT wave power, and $k_{||} = \omega/V_{ph||}$ is the parallel wave number. $V_{ph||} + V_{trap}$ is overplotted as a dashed curve in Figure 2g, which approaches to the beam, supporting that the beam is likely produced by whistler waves through nonlinear Landau resonance.

In the magnetopause reconnection context, electrostatic waves driven and modulated by whistler have been reported (J. Li et al., 2018). They mainly discussed an event in the magnetospheric separatrix region, where whistler originates from anisotropy of hot magnetospheric electrons. The $V_{ph||}$ is around 2×10^4 km/s above local v_{te}, such that the dominant secondary electrostatic wave is Langmuir wave (An et al., 2019). Our event, as well as an event mentioned in J. Li et al. (2018), occurs in the vicinity of the current sheet mid-plane, where whistler arises from the anisotropy of energized magnetosheath-origin electrons in the reconnection exhaust. The corresponding $V_{ph||}$ (a few thousand km/s) is comparable to v_{te}, which theoretically excites electron beam/acoustic mode waves at a fraction of f_{pe} (An et al., 2019). J. Li et al. (2018) observed waves slightly below f_{pe}; our event has occasions of waves slightly below f_{pe} and also at lower frequencies just above f_{pi}.

3.3. Electron Beam Modes and Cyclotron Waves in LHWs

Modulations of electrostatic waves are also found inside LHWs. Figure 3 (left) shows MMS3 observations in the magnetospheric side separatrix region around the density gradient (Figure 3a). LHWs are present mainly below f_{lh}, and extend to higher frequencies in the most intense intervals near 09:52:07 UT (Figures 3e and 3f). We find that separate high-frequency electrostatic waves mainly along $E_{||}$ are present, seen in the waveform that co-exist with $E_{\perp}$ of LHWs (Figure 3c). Their power spectrum is extracted by plotting $|E_{||}|^2 - |E_{\perp}|^2$ (Figure 3d), mainly at $f_{pi} < f < f_{pe}$. The electron $v_{||}$ spectrogram (Figure 3g) exhibits beams. Persistent intense beams at $v_{||}$>0 like those around 09:52:06.7–09:52:07.0 UT, with an example distribution in Figure 3i, are possible magnetosheath electrons moving away from the X-line as the outflow. Later in the lower-density region, the less intense beams repeatedly change directions, also seen in 2D distributions (Figures 3j and 3k).

It has been reported that large-amplitude $E_{||}$ exist in LHWs (e.g., Ergun et al., 2019). We further analyze that high-frequency $E_{||}$ waves may be modulated by LHWs, readily suggested by wave power enhancements that are discrete in time. The recurrence frequency is quantified with the waveform filtered at 0.3–33 kHz during 09:52:06.7–09:52:07.1UT inside the most intense LHWs (Figure 3h). $E_{||}$ wave packets are present with amplitudes up to ~60 mV/m. We identify the envelops of the wave packets (black curve) and extract their maxima

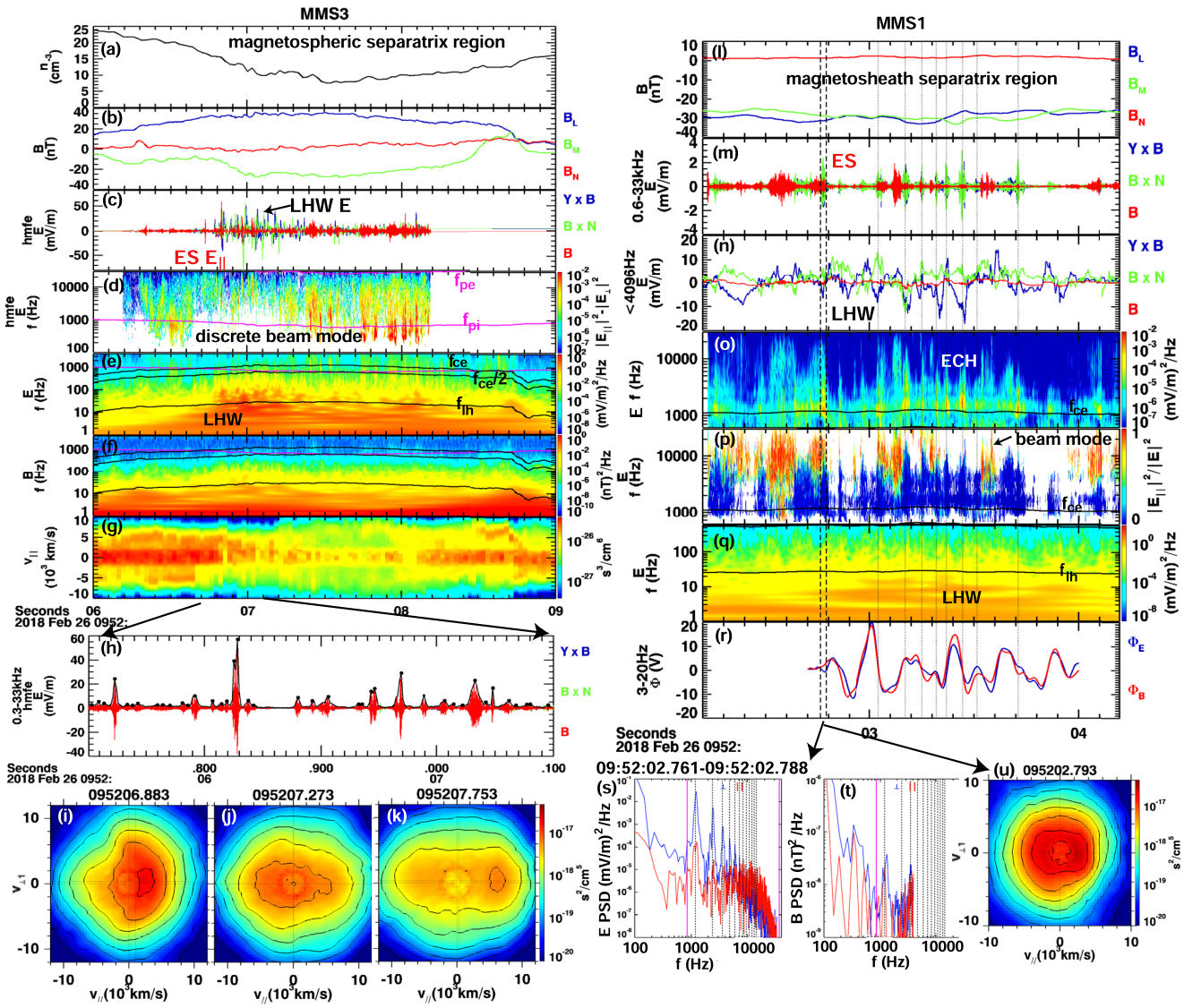

Figure 3. Left: parallel electrostatic waves modulated by lower-hybrid waves (LHWs) in the magnetospheric separatrix region. (a) Electron density; (b) magnetic field; (c) AC electric field; (d) power spectrum of $|E_{||}|^2 - |E_{\perp}|^2$ showing enhancements of parallel electrostatic waves; (e) ***E*** power spectrum at low frequencies showing LHWs; (f) ***B*** power spectrum; (g) electron $v_{||}$ spectrogram; (h) filtered electric field waveform showing $E_{||}$ waves (red); black curve: envelop of the wave; black dots: extracted maxima of the envelops showing a recurrence rate in the LHW frequency range. (i–k) Example electron distributions showing field-aligned beams with varying directions. Right: perpendicular electron cyclotron harmonic (ECH) waves modulated by LHWs in the magnetosheath separatrix region. (l) Magnetic field; (m and n) high- and low-frequency electric field waveforms; (o and p) ***E*** power spectrum and $|E_{||}|^2/|E|^2$ showing modulated perpendicular ECH and additional parallel waves. (q) Low-frequency electric field power spectrum showing LHWs. (r) LHW potential, with ECH enhancements at potential slopes. (s and t) Electric and magnetic field FFT spectra for the interval between vertical dashed lines in (l–r). The corresponding electron distribution exhibits a loss cone at $v_{||} > 0$ (u).

(black dots, required to be >2 mV/m). The reciprocal of intervals between the adjacent maxima are calculated to estimate the recurrence frequency. With 40 identified maxima, the median recurrence frequency is 131 Hz, and the 25% and 75% quartiles are 73 and 164 Hz, respectively. The magnetic field power for LHWs extends to about 300 Hz; the perpendicular electric field power sometimes extends to f_{ce} ~1,000 Hz, and during the analyzed interval, $E_{\perp}$ and $E_{||}$ powers become comparable around 300 Hz (not shown). Thus, we may consider LHWs to be mainly at below 300 Hz. The values of the recurrence frequencies of high-frequency $E_{||}$ waves well lie in the range of the high-frequency part of LHWs, indicating modulations of $E_{||}$ waves by LHWs.

The modulation is likely achieved through generating field-aligned electron beams and exciting electron beam mode waves. LHWs typically have quasi-perpendicular propagations with non-zero $k_{||}$, and the associated $E_{||}$ may modulate and resonate with electrons (e.g., Cairns & McMillan, 2005; Graham et al., 2019; Ng et al., 2023; Ren

et al., 2022; Wang et al., 2021). Therefore, LHWs may modify the distribution near their V_{phll} and excite secondary parallel waves, in a similar way with whistlers. In addition, LHWs produce diffusion for plasmas across boundaries (e.g., Graham et al., 2022; Le et al., 2017; Price et al., 2017), where field-aligned beams can be produced (Le et al., 2018). We infer that electron beams with positive/negative $v_{||}$ (not necessarily near V_{phll} of LHWs) may be generated during the diffusion process, and the beams excite electrostatic waves. We select a few wave packets during 09:52:07.5–09:52:08.2 UT, where the $E_{||}$ waves extend to lower frequencies around f_{pi}, and the "dce" data product captures most of the wave power. Through the interferometry analysis, we find that the time delay of fluctuations between pairs of probes cannot be easily identified by eye, and the automatic correlation analysis suggests a time delay at the order of 1/50 of the data resolution, corresponding to V_{ph} of ∼6,000 km/s (not shown). Such a result is not quantitatively reliable, but it indicates a fast V_{ph}, which is close to the observed electron beam speed of 7,000–8,000 km/s and much greater than the ion thermal speed of ∼350 km/s. Waves around 09:52:07 UT have even higher frequencies and are expected to have larger V_{ph}. Therefore, these fast waves are likely driven by the electron beam mode, with possible thermal effects but without much contribution from ions (e.g., Norgren et al., 2015).

LHW-modulated high-frequency waves are also observed in the magnetosheath separatrix region with large $B_L < 0$ (Figure 3, right). Waveforms show high-frequency waves (Figure 3m) in the midst of LHWs (dominant fluctuations in Figure 3n). LHWs are mainly below f_{lh} ∼25 Hz (Figure 3q), while high-frequency waves are mainly above f_{ce} (Figures 3o and 3p). High-frequency $E_{\perp}$ waves exhibit harmonic features, possibly ECH waves. ECHs have been reported in the magnetosheath separatrix region (Zhou et al., 2016). The FFT spectra of electric and magnetic fields for an example interval between vertical dashed lines are shown in Figures 3s and 3t. The harmonics are right at integers of f_{ce} up to $6f_{ce}$ in electric fields, and one peak can be seen in magnetic fields at $1f_{ce}$, indicating a weak electromagnetic component. Additional broadband $E_{||}$ waves are present at higher frequencies than ECH and below f_{pe}. The electron distribution (Figure 3u) that covers the interval of this wave burst shows a loss cone feature (or perpendicular anisotropy) at $v_{||} > 0$. The spacecraft was at +L side of the X-line at this time, so energetic electrons moving away from the X-line are at $v_{||} < 0$, causing the asymmetry between field-aligned directions (Chen et al., 2016; Fuselier et al., 2011). ECHs are likely excited by loss cone distributions.

ECH wave powers are modulated (Figure 3o): seven bursts show up during ∼0.5 s at 09:52:03.02–09:52:03.52 UT, corresponding to a modulation frequency of 14 Hz in the LHW range. We further calculate the LHW potential in Figure 3r using the method of Norgren et al. (2012), which shows that ECH enhancements (marked by vertical dotted lines) tend to occur at the slopes of the potential, corresponding to peak wave electric fields that possibly drives electron vortices in LHWs (e.g., Chen et al., 2020; Ergun et al., 2019). These gyro-scale potential structures may inflate/compress electron distributions and generate non-gyrotropic features (e.g., Chen et al., 2020; Wang et al., 2021). We infer that the LHW structures modify the loss cone electron distributions in the magnetosheath separatrix region, possibly changing the phase-space gradient of distributions, and modulate ECHs.

4. Summary and Discussions

Based on MMS observations of one magnetopause reconnection diffusion region crossing, we identify widely presented electrostatic waves in different sub-regions. We analyze the wave and plasma properties, and find their associations with lower-frequency waves. The findings are summarized in Figure 1k.

1. Parallel electron beam/acoustic mode waves driven and modulated by whistler are observed in the vicinity of the mid-plane. Adding to J. Li et al. (2018), with their finding about the Langmuir wave in whistler near the magnetospheric separatrix (included in Figure 1j), we further complete the regimes of whistler and the associated secondary waves in the context of magnetopause reconnection.
   Electron distributions in the whistler interval (Figure 2n) have multiple non-Maxwellian features: perpendicular anisotropy of a background population, parallel elongation of electrons with small $v_{\perp}$, and a parallel beam. They may lead to ambiguities about whether each feature is responsible for wave excitation or produced by the waves. In this case, we interpret that the background anisotropy excites whistler, and the beam is produced or at least modulated by Landau resonance with whistler, while beams are unlikely to play a significant role in exciting whistler waves. The DC structure of reconnection can also generate uni-directional electron beams due to changes of the magnetic field topology plus additional acceleration, which may excite whistler waves (e.g., Wang et al., 2022, and references therein). Such reconnection-generated beams are magnetosheath

electrons expected to have high intensities and move toward the magnetosphere (anti-parallel in this case), in a region very close to the X-line. When the low-$v_\perp$ part exhibits a roughly symmetric distribution between $v_{||} > 0$ and $v_{||} < 0$ sides like in Figure 2g (especially after ~09:52:09.5 UT), it is likely that electrons have bounced back and forth in the reconnection exhaust, and the distribution looks flat-topped or with some minor beam features. Therefore, the $v_{||}>0$ beam around 09:52:09.2–09:52:09.4 UT that is clearly asymmetric from the $v_{||} < 0$ side is probably generated by the whistler wave, and the quantitative agreement between the beam speed with the estimated whistler $V_{phl|} + V_{trap}$ further supports this scenario. At later time the overall symmetric distributions with beam features are possibly generated by the DC reconnection structure, and the beams can be modulated through interactions with whistler to generate secondary waves. Even if the beam already exists before whistler, the beam-generated whistler through Landau resonance is expected to be highly oblique, broadband, and quasi-electrostatic, so the observed narrow-band, electromagnetic whistler waves with small θ_{kB} are not generated through the beam Landau resonance; the observed beam has a weak anisotropy, so it cannot excite whistler through cyclotron resonance, either.

2. Analogous to the idea for whistler, we find that LHWs can also modulate high-frequency waves. In LHWs near both magnetospheric and magnetosheath side separatrices, high-frequency wave powers are periodically enhanced with recurrence frequencies in the range of the LHW frequency. On the magnetospheric side, field-aligned electron beams that change directions over time are observed. We infer that LHWs may periodically scatter and produce these beams as they diffuse the density gradient, and the beams excite electron beam mode waves. On the magnetosheath side, ECHs tend to occur at the slopes of LHW potentials. We infer that LHWs modify the loss cone distribution in the separatrix region and modulate ECHs. The exact dynamics about LHW modulations still acquire a better understanding. The presented event is around a secondary EDR, and it is not yet clear whether the LHW modulated waves have any relations to the EDR or they represent a feature that develops at separatrices far downstream.

This event helps us step forward on building a map of waves in reconnection regions, learning about the applicable wave regimes and understanding the coupling of different processes in reconnection. The direct coupling between electromagnetic waves (whistler and LHWs) and electrostatic waves (beam-mode and ECH waves) provides an important channel to convert energy stored in larger spatial scales to smaller spatial scales and to thermal electron heating, assisting in achieving the energy dissipation in reconnection. Although we here emphasize the electrostatic waves modulated by lower-frequency waves, the reconnection structure can also generate distributions that directly excite electrostatic waves as mentioned in Section 1. Such isolated wave packets are also observed in the EDR of the present event, and we will leave the detailed discussions in a separate study. We expect that more systematic and statistical studies of electrostatic waves in reconnection will help consolidate our understanding and solve the open questions.

Data Availability Statement

MMS data are available at https://lasp.colorado.edu/mms/sdc/public/about/browse-wrapper/.

Acknowledgments
SW thanks Dr. Hua-Sheng Xie for helpful discussions on linear instability analyses, Dr. Chao Yue for suggestions on paper presentations, and Dr. Yong-Fu Wang for wave analyses. Research at PKU is supported by "The Fundamental Research Funds for the Central Universities, Peking University" No. 7100604293.

References

An, X., Bortnik, J., & Zhang, X. J. (2021). Nonlinear Landau resonant interaction between kinetic Alfvén waves and thermal electrons: Excitation of time domain structures. *Journal of Geophysical Research: Space Physics*, *126*(1), e2020JA028643. https://doi.org/10.1029/2020JA028643

An, X., Li, J., Bortnik, J., Decyk, V., Kletzing, C., & Hospodarsky, G. (2019). Unified view of nonlinear wave structures associated with whistler-mode chorus. *Physical Review Letters*, *122*(4), 045101. https://doi.org/10.1103/PhysRevLett.122.045101

Burch, J. L., Dokgo, K., Hwang, K. J., Torbert, R. B., Graham, D. B., Webster, J. M., et al. (2019). High-frequency wave generation in magnetotail reconnection: Linear dispersion analysis. *Geophysical Research Letters*, *46*(8), 4089–4097. https://doi.org/10.1029/2019GL082471

Cairns, I. H., & McMillan, B. F. (2005). Electron acceleration by lower hybrid waves in magnetic reconnection regions. *Physics of Plasmas*, *12*(10), 102110. https://doi.org/10.1063/1.2080567

Chen, L.-J., Hesse, M., Wang, S., Gershman, D., Ergun, R., Pollock, C., et al. (2016). Electron energization and mixing observed by MMS in the vicinity of an electron diffusion region during magnetopause reconnection. *Geophysical Research Letters*, *43*(12), 6036–6043. https://doi.org/10.1002/2016GL069215

Chen, L.-J., Wang, S., Le Contel, O., Rager, A., Hesse, M., Drake, J., et al. (2020). Lower-hybrid drift waves driving electron nongyrotropic heating and vortical flows in a magnetic reconnection layer. *Physical Review Letters*, *125*(2), 025103. https://doi.org/10.1103/PhysRevLett.125.025103

Dokgo, K., Hwang, K.-J., Burch, J. L., Yoon, P. H., Graham, D. B., & Li, W. (2020a). The effects of upper-hybrid waves on energy dissipation in the electron diffusion region. *Geophysical Research Letters*, *47*(19), e2020GL089778. https://doi.org/10.1029/2020GL089778

Dokgo, K., Hwang, K.-J., Burch, J. L., Yoon, P. H., Graham, D. B., & Li, W. (2020b). High-frequency waves driven by agyrotropic electrons near the electron diffusion region. *Geophysical Research Letters*, *47*(5), e2020GL087111. https://doi.org/10.1029/2020gl087111

Ergun, R., Tucker, S., Westfall, J., Goodrich, K., Malaspina, D., Summers, D., et al. (2016). The axial double probe and fields signal processing for the MMS mission. *Space Science Reviews*, *199*(1–4), 167–188. https://doi.org/10.1007/s11214-014-0115-x

Ergun, R. E., Hoilijoki, S., Ahmadi, N., Schwartz, S. J., Wilder, F. D., Drake, J. F., et al. (2019). Magnetic reconnection in three dimensions: Modeling and analysis of electromagnetic drift waves in the adjacent current sheet. *Journal of Geophysical Research: Space Physics*, *124*(12), 10085–10103. https://doi.org/10.1029/2019JA027275

Fuselier, S. A., Gurnett, D. A., & Fitzenreiter, R. J. (1985). The downshift of electron plasma oscillations in the electron foreshock region. *Journal of Geophysical Research*, *90*(A5), 3935–3946. https://doi.org/10.1029/JA090iA05p03935

Fuselier, S. A., Trattner, K. J., & Petrinec, S. M. (2011). Antiparallel and component reconnection at the dayside magnetopause. *Journal of Geophysical Research*, *116*(A10), A10227. https://doi.org/10.1029/2011JA016888

Graham, D. B., Khotyaintsev, Y. V., André, M., Vaivads, A., Divin, A., Drake, J. F., et al. (2022). Direct observations of anomalous resistivity and diffusion in collisionless plasma. *Nature Communications*, *13*(1), 2954. https://doi.org/10.1038/s41467-022-30561-8

Graham, D. B., Khotyaintsev, Y. V., Norgren, C., Vaivads, A., André, M., Drake, J. F., et al. (2019). Universality of lower hybrid waves at Earth's magnetopause. *Journal of Geophysical Research: Space Physics*, *124*(11), 8727–8760. https://doi.org/10.1029/2019JA027155

Graham, D. B., Khotyaintsev, Y. V., Vaivads, A., & Andre, M. (2016). Electrostatic solitary waves and electrostatic waves at the magnetopause. *Journal of Geophysical Research: Space Physics*, *121*(4), 3069–3092. https://doi.org/10.1002/2015JA021527

Graham, D. B., Khotyaintsev, Y. V., Vaivads, A., Norgren, C., André, M., Webster, J. M., et al. (2017). Instability of agyrotropic electron beams near the electron diffusion region. *Physical Review Letters*, *119*(2), 025101. https://doi.org/10.1103/PhysRevLett.119.025101

Gurnett, D. A., & Bhattacharjee, A. (2005). Chapter 8: Electrostatic waves in hot unmagnetized plasma. In *Introduction to plasma physics with space and laboratory applications*. Cambridge University Press.

Jiang, K., Huang, S. Y., Yuan, Z. G., Sahraoui, F., Deng, X. H., Yu, X. D., et al. (2019). The role of upper hybrid waves in the magnetotail reconnection electron diffusion region. *The Astrophysical Journal Letters*, *881*(2), L28. https://doi.org/10.3847/2041-8213/ab36b9

Khotyaintsev, Y. V., Graham, D. B., Norgren, C., & Vaivads, A. (2019). Collisionless magnetic reconnection and waves: Progress review. *Frontiers in Astronomy and Space Sciences*, *6*(70), 1–20. https://doi.org/10.3389/fspas.2019.00070

Khotyaintsev, Y. V., Graham, D. B., Steinvall, K., Alm, L., Vaivads, A., Johlander, A., et al. (2020). Electron heating by Debye-scale turbulence in guide-field reconnection. *Physical Review Letters*, *124*(4), 045101. https://doi.org/10.1103/PhysRevLett.124.045101

Le, A., Daughton, W., Chen, L.-J., & Egedal, J. (2017). Enhanced electron mixing and heating in 3-D asymmetric reconnection at the Earth's magnetopause. *Geophysical Research Letters*, *44*(5), 2096–2104. https://doi.org/10.1002/2017GL072522

Le, A., Daughton, W., Ohia, O., Chen, L. J., Liu, Y. H., Wang, S., & Bird, R. (2018). Drift turbulence, particle transport, and anomalous dissipation at the reconnecting magnetopause. *Physics of Plasmas*, *25*(6), 062103. https://doi.org/10.1063/1.5027086

Le Contel, O., Leroy, P., Roux, A., Coillot, C., Alison, D., Bouabdellah, A., et al. (2016). The search-coil magnetometer for MMS. *Space Science Reviews*, *199*(1–4), 257–282. https://doi.org/10.1007/s11214-014-0096-9

Li, J., Bortnik, J., An, X., Li, W., Russell, C. T., Zhou, M., et al. (2018). Local excitation of whistler mode waves and associated Langmuir waves at dayside reconnection regions. *Geophysical Research Letters*, *45*(17), 8793–8802. https://doi.org/10.1029/2018GL078287

Li, J., Bortnik, J., Li, W., Thorne, R. M., Ma, Q., Chu, X., et al. (2017). Coherently modulated whistler mode waves simultaneously observed over unexpectedly large spatial scales. *Journal of Geophysical Research: Space Physics*, *122*(2), 1871–1882. https://doi.org/10.1002/2016JA023706

Li, W.-Y., Graham, D. B., Khotyaintsev, Y. V., Vaivads, A., André, M., Min, K., et al. (2020). Electron Bernstein waves driven by electron crescents near the electron diffusion region. *Nature Communications*, *11*(1), 141. https://doi.org/10.1038/s41467-019-13920-w

Li, W.-Y., Khotyaintsev, Y. V., Tang, B.-B., Graham, D. B., Norgren, C., Vaivads, A., et al. (2021). Upper-hybrid waves driven by meandering electrons around magnetic reconnection X line. *Geophysical Research Letters*, *48*(16), e2021GL093164. https://doi.org/10.1029/2021GL093164

Lindqvist, P.-A., Olsson, G., Torbert, R., King, B., Granoff, M., Rau, D., et al. (2016). The spin-plane double probe electric field instrument for MMS. *Space Science Reviews*, *199*(1–4), 137–165. https://doi.org/10.1007/s11214-014-0116-9

Liu, Z.-Y., Zong, Q.-G., Rankin, R., Zhang, H., Wang, Y. F., Zhou, X.-Z., et al. (2022). Simultaneous macroscale and microscale wave-ion interaction in near-earth space plasmas. *Nature Communications*, *13*(1), 5593. https://doi.org/10.1038/s41467-022-33298-6

Lu, Q., Wang, S., & Dou, X. (2005). Electrostatic waves in an electron-beam plasma system. *Physics of Plasmas*, *12*(7), 072903. https://doi.org/10.1063/1.1951367

Ng, J., Yoo, J., Chen, L.-J., Bessho, N., & Ji, H. (2023). 3D simulation of lower-hybrid drift waves in strong guide field asymmetric reconnection in laboratory experiments. *Physics of Plasmas*, *30*(4), 042101. https://doi.org/10.1063/5.0138278

Norgren, C., André, M., Graham, D., Khotyaintsev, Y. V., & Vaivads, A. (2015). Slow electron holes in multicomponent plasmas. *Geophysical Research Letters*, *42*(18), 7264–7272. https://doi.org/10.1002/2015GL065390

Norgren, C., Vaivads, A., Khotyaintsev, Y. V., & Andre, M. (2012). Lower hybrid drift waves: Space observations. *Physical Review Letters*, *109*(5), 55001. https://doi.org/10.1103/PhysRevLett.109.055001

Omura, Y., Matsumoto, H., Miyake, T., & Kojima, H. (1996). Electron beam instabilities as generation mechanism of electrostatic solitary waves in the magnetotail. *Journal of Geophysical Research*, *101*(A2), 2685–2697. https://doi.org/10.1029/95JA03145

Pollock, C., Moore, T., Jacques, A., Burch, J., Gliese, U., Saito, Y., et al. (2016). Fast plasma investigation for magnetospheric multiscale. *Space Science Reviews*, *199*(1–4), 331–406. https://doi.org/10.1007/s11214-016-0245-4

Price, L., Swisdak, M., Drake, J. F., Burch, J. L., Cassak, P. A., & Ergun, R. E. (2017). Turbulence in three-dimensional simulations of magnetopause reconnection. *Journal of Geophysical Research: Space Physics*, *122*(11), 11086–11099. https://doi.org/10.1002/2017JA024227

Ren, Y., Dai, L., Wang, C., & Lavraud, B. (2022). Parallel electron heating through Landau resonance with lower hybrid waves at the edge of reconnection ion jets. *The Astrophysical Journal*, *928*(1), 5. https://doi.org/10.3847/1538-4357/ac53fb

Russell, C., Anderson, B., Baumjohann, W., Bromund, K., Dearborn, D., Fischer, D., et al. (2016). The magnetospheric multiscale magnetometers. *Space Science Reviews*, *199*(1–4), 189–256. https://doi.org/10.1007/s11214-014-0057-3

Samson, J. C., & Olson, J. V. (1980). Some comments on the descriptions of the polarization states of waves. *Geophysical Journal International*, *61*(1), 115–129. https://doi.org/10.1111/j.1365-246X.1980.tb04308.x

Torbert, R. B., Russell, C. T., Magnes, W., Ergun, R. E., Lindqvist, P. A., LeContel, O., et al. (2016). The FIELDS instrument suite on MMS: Scientific objectives, measurements, and data products. *Space Science Reviews*, *199*(1–4), 105–135. https://doi.org/10.1007/s11214-014-0109-8

Wang, S., Bessho, N., Graham, D. B., Le Contel, O., Wilder, F. D., Khotyaintsev, Y. V., et al. (2022). Whistler waves associated with electron beams in magnetopause reconnection diffusion regions. *Journal of Geophysical Research: Space Physics*, *127*(9), e2022JA030882. https://doi.org/10.1029/2022JA030882

Wang, S., Chen, L.-J., Bessho, N., Ng, J., Hesse, M., Graham, D. B., et al. (2021). Lower-hybrid wave structures and interactions with electrons observed in a 3D symmetric reconnection simulation with zero guide field. *Physics of Plasmas*, *28*(7), 072102. https://doi.org/10.1063/5.0054626

Wang, S., Chen, L.-J., Ng, J., Bessho, N., Le, G., Fung, S. F., et al. (2020). A case study of nonresonant mode 3-s ULF waves observed by MMS. *Journal of Geophysical Research: Space Physics*, *125*(11), e2020JA028557. https://doi.org/10.1029/2020JA028557

Wilder, F. D., Ergun, R. E., Hoilijoki, S., Webster, J., Argall, M. R., Ahmadi, N., et al. (2019). A survey of plasma waves appearing near dayside magnetopause electron diffusion region events. *Journal of Geophysical Research: Space Physics*, *124*(10), 7837–7849. https://doi.org/10.1029/2019JA027060

Zhang, X.-J., Chen, L., Artemyev, A. V., Angelopoulos, V., & Liu, X. (2019). Periodic excitation of chorus and ECH waves modulated by ultra-low frequency compressions. *Journal of Geophysical Research: Space Physics*, *124*(11), 8535–8550. https://doi.org/10.1029/2019JA027201

Zhou, M., AshourAbdalla, M., Berchem, J., Walker, R. J., Liang, H., El-Alaoui, M., et al. (2016). Observation of high-frequency electrostatic waves in the vicinity of the reconnection ion diffusion region by the spacecraft of the Magnetospheric Multiscale (MMS) mission. *Geophysical Research Letters*, *43*(5), 4808–4815. https://doi.org/10.1002/2016GL069010